SMHI

No 93, November 2000

Reports Meteorology and Climatology

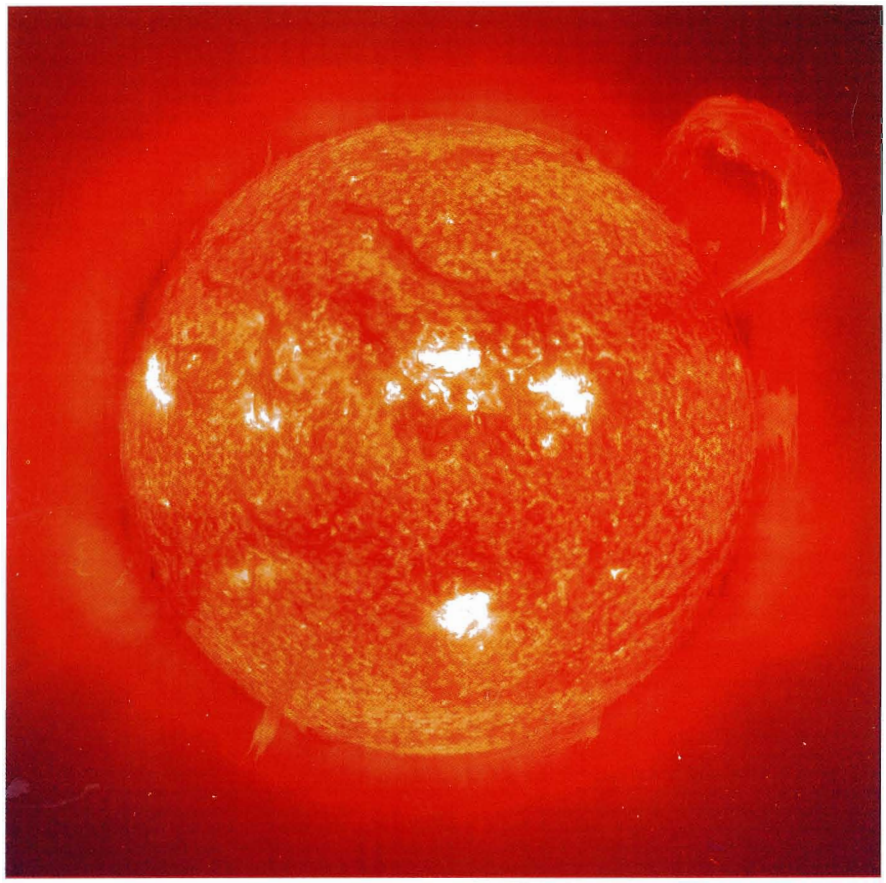

Using the sun to check some weather radar parameters

Tage Andersson

Cover: The sun emits radiation also in the micro-wave frequencies. The intensity of this radiation is not constant, but generally varies only slowly and is monitored by solar observatories. The image, from NASA, Sep. 14, 1999, shows a huge, handleshaped prominence, that is a cloud of relatively cold plasma. Disturbances of this kind and sunspots have an impact upon the intensity of the sun's micro-wave radiation.

RMK
No 93, November 2000

Using the sun to check some weather radar parameters

Tage Andersson

Report Summary / Rapportsammanfattning

Issuing Agency/Utgivare	Report number/Publikation
Swedish Meteorological and Hydrological Institute S-601 76 NORRKÖPING Sweden	RMK No. 93
	Report date/Utgivningsdatum November 2000

Author (s)/Författare

Tage Andersson

Title (and Subtitle/Titel)

Using the sun to check some weather radar parameters

Abstract/Sammandrag

Precipitation monitoring is a main task for weather radar applications. In quantitative applications, as estimation of the rain rate, the fundamental quantity is the measurement of the intensity of the return signal strength, giving the so called *reflectivity factor*, or *reflectivity*, which is the main parameter for those estimates. The calibration of weather radars for this purpose has been a main task in radar meteorology since the first attempts of estimating rain rates in the early 1950ies. In spite of this there is still no international accepted procedure for this calibration and each manufacturer has his own calibration scheme.

There is evidently a need for a target to calibrate against, which is common for all radars and easily accessible. This points towards astronomical targets. The moon is such a possible target, though the echo from it is too weak for routine calibrations. The sun emits radiation in the radar frequencies. These signals are already widely used to determine the orientation of the antenna (azimuth and elevation angle). The intensity of the radiation in these frequencies is not constant, but is measured by some observatories and may be used as a calibration source.

The present work is an attempt to design a calibration or checking procedure that can be used when the radar is working operatively.

Key words/sök-, nyckelord

Weather radar calibration, the sun as a radiation source.

Supplementary notes/Tillägg	Number of pages/Antal sidor	Language/Språk
	30	English

ISSN and title/ISSN och titel

0347-2116 SMHI Reports Meteorology Climatology

Report available from/Rapporten kan köpas från:

SMHI
S-601 76 NORRKÖPING
Sweden

Content

USING THE SUN TO CHECK SOME WEATHER RADAR PARAMETERS

Tage Andersson
Swedish Meteorological and Hydrological Institute
S-60176 Norrköping

1. Abstract

Precipitation monitoring is still a main task for weather radar applications. In quantitative applications, as estimation of the rain rate, the fundamental quantity is the measurement of the intensity of the return signal strength, giving the so called *reflectivity factor*, or *reflectivity*, which is the main parameter for those estimates. The calibration of weather radars for this purpose has been a main task in radar meteorology since the first attempts of estimating rain rates in the early 1950ies. In spite of this there is still no international accepted procedure for this calibration and each manufacturer has his own calibration scheme.

One radar has a limited area of surveillance. In order to increase the radar surveillance area, composite images or image mosaics are built, using data from several radars (national or multinational). The composite images have often revealed that neighbouring radars may give different reflectivity values in overlapping areas also where their beams occupy approximately the same atmospheric volumes, that is where the beams intersect halfway between the radars (assuming free horizon, same elevation angle and beam-width and so on). Differences appear not only between radars of different types and sites, but also between radars of the same type. The differences often exceed a few dB, occasionally surpassing 5 dB (Pratte 1995, Dahlberg 1996), though the repeatability of a single measurement is much better. As an example, in the NORDRAD it was found that reflectivities from Swedish and Finnish weather radars could differ by more than 10 dBz in their overlapping areas. (An error of 10 dBz gives an error factor of about 4 in rain rate). Dahlberg (1996) showed that most of these differences were due to software errors in both systems. The accuracy claimed, and generally promised by the manufacturers, is about 1 dBz.

There is evidently a need for a target to calibrate against, which is common for all radars and easily accessible. This points towards astronomical targets. The moon is such a possible target, though the echo from it is too weak for routine calibrations. The sun emits radiation in the radar frequencies. These signals are already widely used to determine the orientation of the antenna (azimuth and elevation angle). The radiation in these frequencies are measured by some observatories and may be used as a calibration source, Whiton et al (1976), Frush (1984).

The present work is an attempt to design a calibration or checking procedure that can be used when the radar is working operationally. It was found that the ordinary

scanning schemes and the angle accuracy did not permit a satisfactory 'hit' of the sun, Therefore I had to introduce some (about 10) extra antenna elevations. These are as close to each other as possible (0.2° with our radars). Then generally one elevation angle coincides (±0.1°) with the sun's elevation angle at least twice a day. The resolution in azimuth is 0.85°. Since the sun generally is seen in two consecutive azimuths, interpolation is possible in order to compute the flux received if the antenna had been pointing exactly into the sun. The probable accuracy of the method is about or slightly better than 1 dB. This method also permits a check of the azimuth and elevation angles given by the radar.

Technical data for the Ericsson Doppler weather radars are given in the appendix.

Observations of solar flux have been obtained from the Australian Space Forecast Center and the Dominion Radio Astrophysical Observatory, Canada.

2. The pilot study

The idea to this project originated in observations of the sun echo on radar images of the type used in the weather service. The sun emission gives a characteristic echo, whose intensity seems constant with time. Since the calibration of the intensity signal still is a problem, the sun could perhaps be used as a standard target, which is easily observed. My first observations used only such pictures, or digital recordings, of the intensity of the sun echo at the maximum range of the radar in the non-Doppler mode (240 km). The elevation angles were low, about 1°, simply since the scanning strategy included several scans at such elevations, and the sun was often observed. The maximum of the observed signals at a range of, or close to, the maximum range were recorded. The results are given in Fig. 1. Most conspicuous is a rapid drop of about 5 dB. This jump was caused by a soft-ware change due to the detection of an error giving 5 dB too high values (Dahlberg, 1996). Otherwise the span of the values is

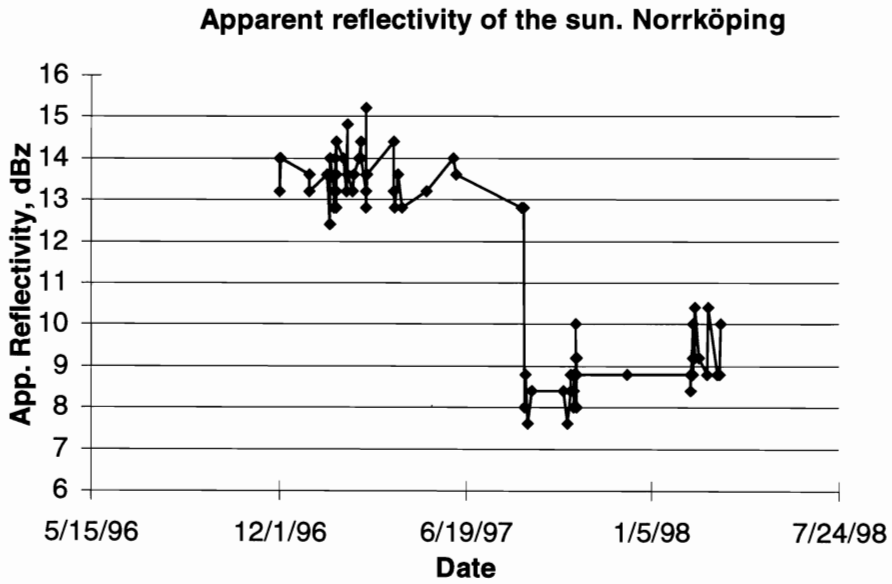

Fig. 1. Observed 'reflectivity' of the sun at 'range' 240 km with antenna elevation angles of about 1 °. The 5 dB jump is caused by a modification of the software, see text.

about 3 dB. Using such low elevation angles is not a good choice, since the attenuation of the atmosphere is serious, as well as the bending of the rays in the vertical plane.

Another difficulty is that, due to the resolution in azimuth (0.86°) it is impossible to decide how 'exact' the hit of the sun (angular diameter 0.53°) is.

The main objection raised has been that the intensity of the sun radiation, the solar flux, is variable in this frequency. However, Fig. 1 suggests that the solar flux does not vary much. The variations, apart from the 5 dB jump discussed, could well be caused by variations in attenuation and how the radar antenna has been aligned with respect to the sun.

3. The emission from the sun

The sun emits radio energy over the whole radio spectrum. This emission consists of three main components (Croom, 1973)

- The quiet sun emission
- The slowly varying component
- Bursts

The quiet sun emission is the unpolarised thermal emission from the solar atmosphere. It is not constant, but varies over an 11 years period, corresponding to the sunspot cycle.

The slowly varying component varies from day to day and originates near sunspot regions. The individual regions have a diameter of a few hundreds of degrees. Several such regions can occur at independent locations on the solar disc. The variation arises because of decay and birth of regions. Individual regions may persist for months. Due to the rotation of the sun, the persisting regions give a 27 days periodicity. Due to the dynamics of such spots, day-to-day variations are superposed upon this periodicity.

The Solar Bursts are the most violent variations in the solar radio emission. Bursts usually occur above the sunspot regions responsible for the slowly varying component and are generally associated with solar optical flares (a flare is a sudden eruption of energy on the solar disk, lasting from minutes to hours). The sunspot regions are normally only a few hundreds of degrees in diameter. In spite of their small size they can cause the integrated emission from the solar disc to increase with about 20 dB at the C band. Such strong bursts are only expected to occur two to three times per 11 year solar cycle. Most bursts cause radiation increases below 2 dB.

Observed solar fluxes from Learmonth, Australia, and Carrington, Canada, are shown in Fig. 2. The data is obtained via internet, and are measurements once a day, from Learmonth at about 4 UTC and from Carrington about 22 UTC the preceding day. As to Learmonth also data which are marked as questionable are included. The unit is the so called Solar Flux Unit, sfu.

$$1\ sfu = 10^{-22} W\, m^{-2} Hz^{-1}$$

The values are given in dB with respect to 1 sfu (dB=10 * ^{10}log(sfu)). The span of the C band values is about 2 dB.

During my observations I have noticed one solar burst. This was possible to observe on some of our radars, simply by observing at an elevation angle close to the sun. It is only by coincide this was possible, and it is not probable that we got good hits of the sun, and our recordings must therefore be considered only approximate, Nevertheless, the burst is evident in Fig. 3. The Learmonth data are actually available with a 1 minute time resolution, and flagged when considered doubtful due to bursts or other causes. One drawback with using data from an observatory on the 'opposite half-sphere is that data is available during much of our daytime, since the sun is the

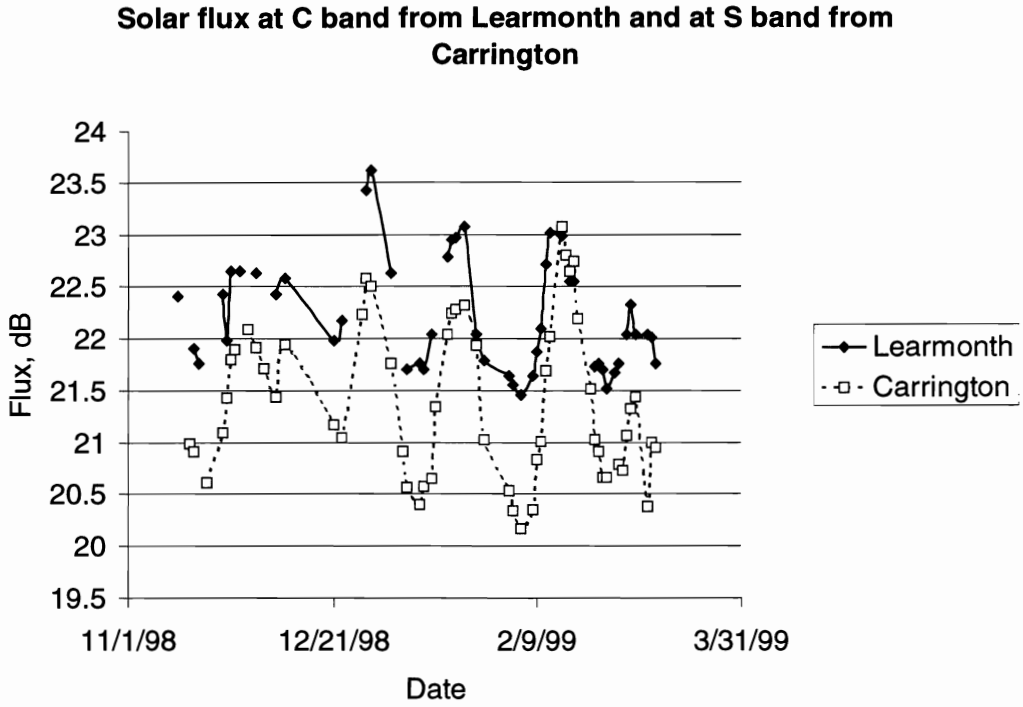

Fig 2. The unit of flux is sfu. The observations are daily, at about maximum sun elevation.

below the horizon at the observatory. However, if we contend ourselves with an accuracy of about 1 dB the sun should suffice.

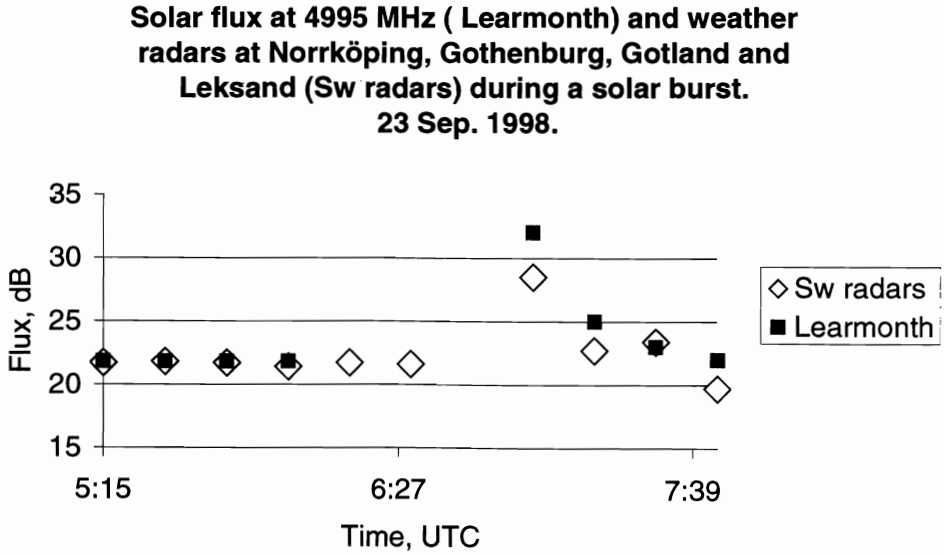

Fig. 3. The solar burst is evident on the Swedish radars.

4. The computation of the sun's 'reflectivity'

When the radar antenna points into the sun, it receives continuos signals from the sun. The signals are located into range gates after the time that has elapsed since the transmitting of a pulse. For each PRT (Pulse repetition Time) the intensity of the sun signal is integrated for each range gate. 6 consecutive range bins are integrated to form every pixel, but only 1 azimuth bin is used. Of these 120 range pixels, the ones closest to the antenna are always contaminated by ground echos, and sometimes also by other targets, as from precipitation, clear air or birds. Therefore the range gates closest to the antenna cannot be used to estimate the sun signal. How far out one has to go depends on the antenna elevation angle used. For the lowest such angles we have used for the quantitative study, 7°, the closest range pixel used is generally no 30. This corresponds to a range of 60 km and a height of the centre of the beam of 7.5 km. Precipitation echos may appear at this height, but for the data used I have checked that no such echos were present. In order to get the reflectivity estimates comparable, they have to refer to a common range. The maximum range of the radar, the range 120 pixels, corresponding to 240 km, has been used. The corrections for beam broadening and attenuation by the atmospheric gases have to be removed with the radar equation. The attenuation due to precipitation is negligible for signals as weak as the sun signal. Writing the weather radar equation (2) in the form

$p_r = const*Z/(r^2 L_a)$
gives
$10*\log p_r = 10*\log const + dBz - 20*\log r - 10*\log L_a$
where $10*\log L_a = 0.016*r$
gives

$$dBz_{240} = dBz_r + 20*\log(240/r) + 0.016*(240-r) \qquad (1)$$

where

r	range in km
dBz_{240}	reflectivity at range 240 km
dBz_r	reflectivity at range r
0.016	coefficient of attenuation for atmospheric gases, two-way, dB/km

An example of such data is shown in Fig. 4. Since the sun signal is only a few dB above the minimum detectable signal it may occur that some range bins lack echos even when the antenna is directed towards the solar disc. When the antenna is pointing to the outer part of the sun or slightly beside it, several pixels lack echos, Fig. 5, and the frequency distribution of the reflectivities are bounded to the left, Fig. 7. The number of answers may be used as a rough estimate of how well the antenna is aligned into the sun. If the hit is good, there are generally answers in all range gates, Fig. 4, and the frequency distribution of the reflectivities is symmetric, Fig. 6. Farther out from the sun centre than about 0.2°, the number of answers tends to be below 100% and decreases with the angular distance. However, the number of answers also depends upon the solar flux itself and the sensitivity of the radar. For every scan, which consists of several elevations, the following statistics have been computed for the polar pixels giving sun echos:

av_dBz	*arithmetic average of dBz*
av_z	*arithmetic average of z in dB*
s_dBz	*standard deviation of dBz*
max_z	*maximum value of dBz*
min_z	*minimum value of dBz*
n_e	*number of pixels with echo*
n_0	*number of pixels without echo*

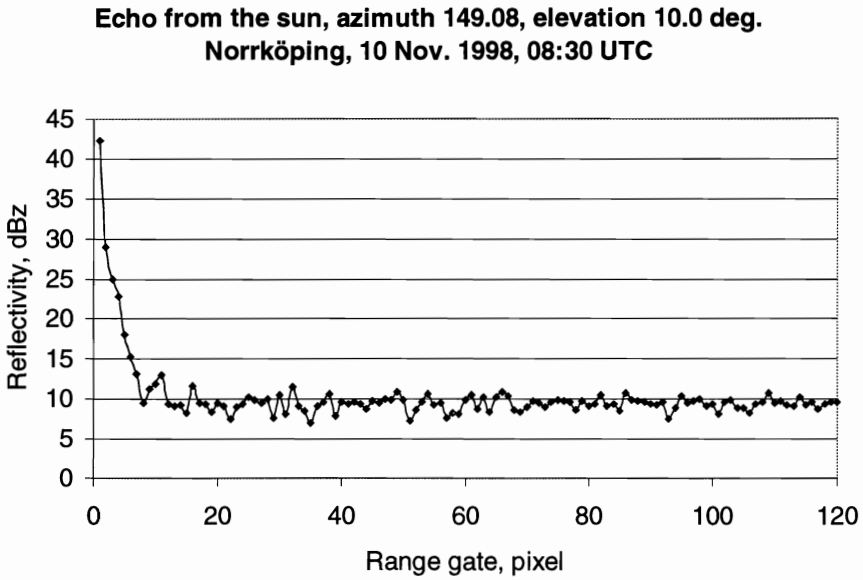

Fig. 4. The pixels closest to the antenna are contaminated by echos which are not due to the sun.

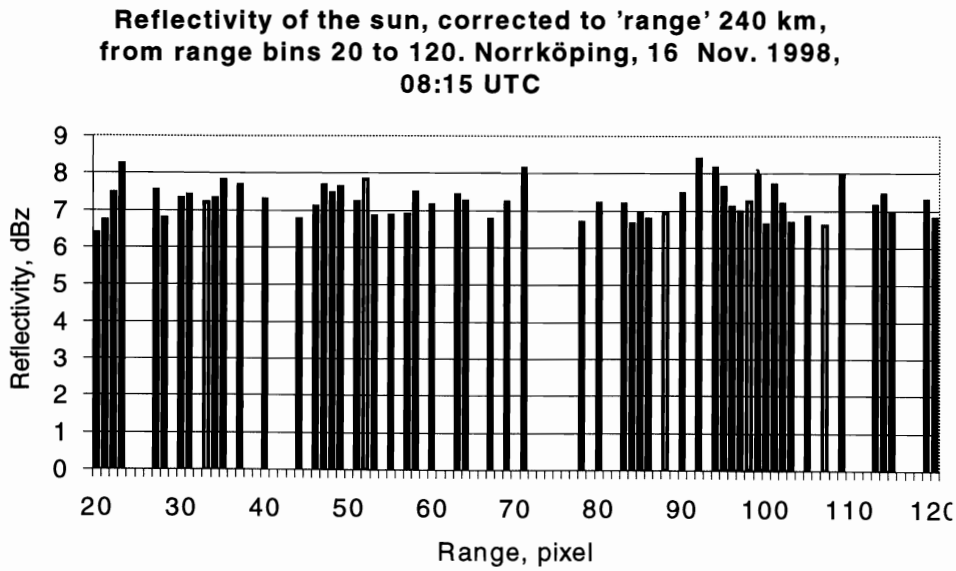

Fig. 5. The sun signal may be too weak to be recorded.

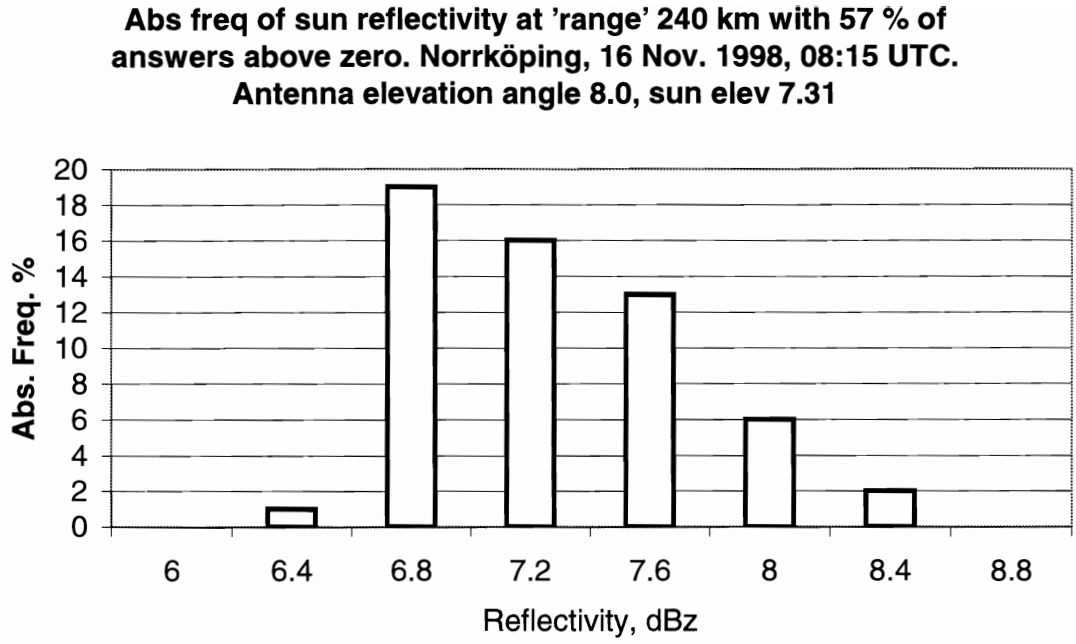

Fig. 6. The distribution is bounded to the left, since the sun signals there are below the minimum detectable signal

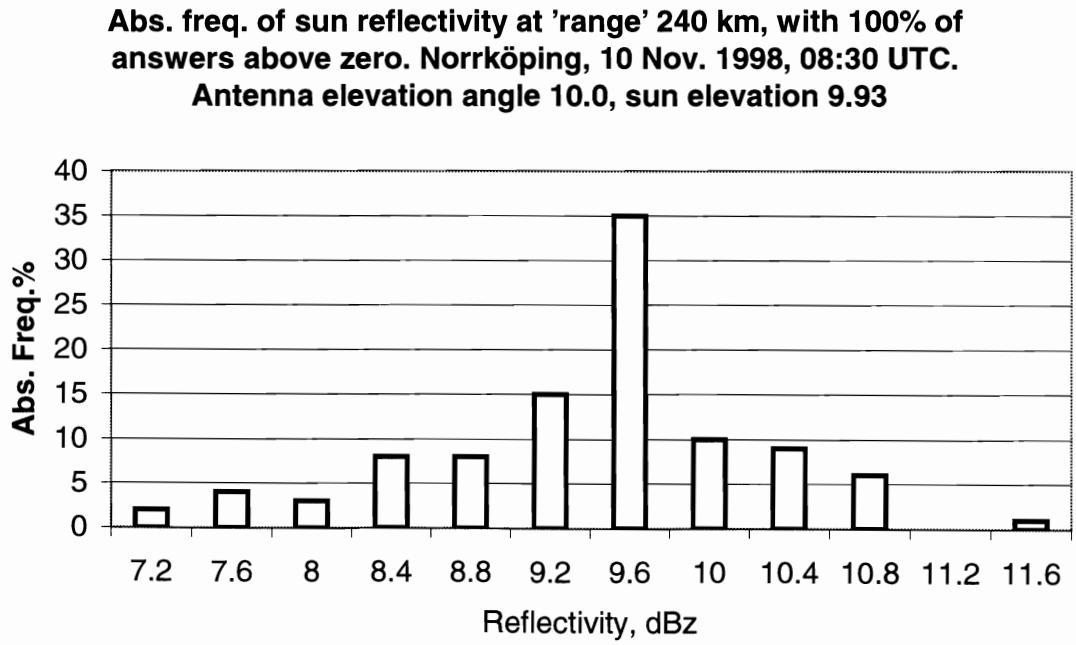

Fig. 7. If the signals are above the minimum detectable signal, the distributions become symmetric.

Table 1 gives an example of the computations performed. The events have been selected so that the sun should be centred in the 'close' elevation angle scan interval

Table 1: Sun echo at different azimuth and elevation angles. The statistics refer to the range pixels 30 to 120

DD-MMM-YY	day-month-year
HH:MI	hour minute in UTC
AZIM	azimuth of the radar, degrees
ELEV	elevation angle of the radar, degrees
no	number of elevation angle
av_dbz	arithmetic average of the dBz values from range r to 120. Generally r=30 range pixels
s_dbz	standard deviation of dBz
n_e	number of range bins with echo
n_0	number of range bins without echo
av_z	arithmetic mean of the Z values, in dB
min_z	minimum of the dBz values
max_z	maximum of the dBz values

NORRKÖPING, sun at azimuth 128.06° elevation 15.64°, at 07:48 UTC

DD-MMM-YYYY	HH:MI	AZIM	ELEV	no	av_dbz	s_dbz	n_e	n_0	av_z	min_z	max_z
9-MAR-1999	07:45	126,81	15,0	9	6,85	0,24	2	89	6,85	6,68	7,02
9-MAR-1999	07:45	126,81	15,2	10	7,19	0,52	27	64	7,22	6,48	8,33
9-MAR-1999	07:45	126,81	15,4	11	6,85	0,23	8	83	6,85	6,65	7,33
9-MAR-1999	07:45	126,81	15,6	12	7,19	0,33	19	72	7,20	6,72	7,84
9-MAR-1999	07:45	126,81	15,8	13	6,79	0,12	3	88	6,79	6,68	6,92
9-MAR-1999	07:45	127,66	15,0	9	7,71	0,72	74	17	7,77	6,52	9,78
9-MAR-1999	07:45	127,66	15,2	10	8,79	0,80	89	2	8,87	6,91	10,73
9-MAR-1999	07:45	127,66	15,4	11	9,41	0,92	91	0	9,51	6,91	11,72
9-MAR-1999	07:45	127,66	15,6	12	9,74	0,86	91	0	9,82	7,20	11,80
9-MAR-1999	07:45	127,66	15,8	13	9,53	0,86	91	0	9,62	6,79	11,77
9-MAR-1999	07:45	127,66	16,0	14	8,57	0,83	90	1	8,65	7,00	10,12
9-MAR-1999	07:45	127,66	16,2	15	7,60	0,75	73	18	7,67	6,66	9,77
9-MAR-1999	07:45	127,66	16,4	16	6,80	-0,40	1	90	6,80	6,80	6,80

The best hit occurred at azimuth 127.66° and elevation 15.6°.

5. The meteorological radar equation

We will use the following notations (mostly as Dahlberg 1996). When convenient, also values of the parameters for the non-Doppler mode of our Ericsson radars are given and if they are assumed constants or determined at the technical calibrations, by routine performed once every year.

P_t	Peak transmitter output power, W		
p_t	Average output power, W	120	calibrated
p_r	Average received power, W		
G	Antenna gain	44.9 dB	constant
A	Antenna effective area, m^2		
Θ	Beam width, radians or ^{o}	0.9°	constant
c	Speed of light, m/s		
τ	Pulse width, microseconds	2.0	constant
λ	Wavelength, m		
f	Transmitted frequency, Hz	5610 MHz	calibrated
L_{tot}	Radar loss	Several terms	
L_a	Attenuation	Several terms	
r	range, m		
Z	Radar reflectivity factor, mm^6/m^3		
dBz	reflectivity	dBz = 10* ^{10}logZ	
$\lvert K \rvert^2$	Index of refraction	0.93	constant
C	radar constant		
PRF	Pulse repetition frequency, s^{-1}	250	constant
PRT	Pulse repetition time, s	1/250	

The meteorological radar equation, as given by Probert-Jones (1962) and Battan (1973) reads,

$$p_r = (\pi^3/1024*ln2) * (P_t * G^2 * \Theta^2 * c * \tau / \lambda^2 * L_{tot}) * (\lvert K \rvert^2 * Z/L_a * r^2) * (10^{-18}) \qquad (2)$$

The factor (10^{-18}) is due to the dimension of Z.

The following discussion of the terms refers to Dahlberg (1996).

The term L_{tot} has four components

L_{wg}	waveguide loss, two-way	1.8 dB	calibrated
L_{rad}	radome loss, two-way	0.4 dB	constant
L_{meth}	method loss	-2.5 dB	constant
L_{det}	detection loss	1.2 dB	constant

$$L_{tot} = L_{wg} + L_{rad} + L_{meth} + L_{det}$$

The attenuation term, L_a, has two components

$L_{air} = 0.016*r$ 0.016 dB/km is the attenuation by clear air, two-way

L_{prec} = attenuation in precipitation	Omitted here since it gives negligible contributions to our measurements.

5.1 Use of the radar equation in our application

The radar gives the dBz value, that is $10 * {}^{10}\log Z$, which we will call the reflectivity.

Assuming an incoming signal independent of range, as the solar signal, the radar will depict such a signal as a range-dependent one, since the range appears as the beam-broadening term $1/r^2$, as well as $1/r$ in the attenuating term, in the radar equation. Note that range, when measuring the solar flux, only is an expression for the time between transmitting a pulse and receiving the sun signal and does not correspond to a geometric distance. If we give the solar signal in Z or dBz, we have to give it at a fixed range. In this work I have used the range of 240 km, that is the maximum range of our radars in the non-Doppler mode.

This reflectivity factor may be read from a PPI, or the data volumes in polar coordinates. For qualitative checks, the dBz read from a PPI may be sufficient, but if we want to make more accurate estimates it must be read from the data volumes, and precautions be taken that the antenna really points into the sun.

Using this dBz value, the meteorological radar equation gives the signal received from the sun. In order to get the flux from the sun, a radar equation for the sun as target must be developed.

5.2 Radar equation for the sun

The relation between the effective antenna area A and the antenna gain G is

$$G = 4\pi * A/\lambda \qquad (3)$$

From this we get the effective area

$$A = G * \lambda/4\pi$$

Assuming that we know G we can thus compute the effective antenna area. Now the sun occupies only part of this area

We assume a Gaussian lobe where the lobe angular radius, $\theta/2$, is $1.17*\sigma$. Introducing $z=\alpha/\sigma$, where α is the angle from the centre of the lobe, the lobe shape is then

$$f(\alpha) = \frac{1}{\sqrt{2\pi}} \exp(-t)$$

where $t=z^2/2$

The area under this curve is

$$\int_{-\infty}^{\infty} f(\alpha)d\alpha = 1$$

The sun only occupies a part of this area

$$f(sun) = \int_{\alpha-sr}^{a+sr} f(\alpha)d\alpha \qquad (4)$$

where sr is the radius of the sun (0.53/2 degrees)

f(sun) is thus a function of the angle to the sun, see Table 2.

Table 2. Effective area of the sun as a function of the angle to the sun

Angle to sun, α, deg.	*Relative area f(sun)*
0.0	*0.51*
0.1	*0.49*
0.2	*0.46*
0.3	*0.41*
0.4	*0.32*
0.5	*0.25*
0.6	*0.18*
0.7	*0.12*
0.8	*0.08*
0.9	*0.05*
1.0	*0.02*

The reason for giving these results is that our equipment does not permit pointing the antenna exactly (say within 0.1^{o}) into the sun. We don't have any hand-wheels for adjusting the antenna until we get the maximum sun signal. If we want to get a 'sun hit' we have to use the astronomic equations to get the sun position, command the antenna to this position and then measure the sun signal. Since we cannot be sure that the antenna is exactly aligned, and the antenna positioning accuracy is of the order of a few tenths of a degree, we cannot be sure that this 'dead reckoning, gives a good hit. However, choosing a time about the maximum sun height gives a good possibility to get the azimuth, and that actually is the method used for positioning the antennas in azimuth. Moreover, the intention of this work is to get a method for a check of some radar parameters that can easily be performed when the radar is running operatively. We thus have to develop a method that gives a fairly good 'sun hits' and from them interpolate the parameters wanted, that is azimuth and elevation angle and signal intensity. Fig. 8 shows the effective area for two azimuth gates, the one closest to the sun and the one next closest. In our computations, generally some range pixels in the next closest azimuth lack observations, since the signal intensity is below the minimum detectable signal. The estimated averages then becomes too high, since the lowest values are missing. To compensate this the effective area of the next closes azimuth may ben increased, Fig. 9.

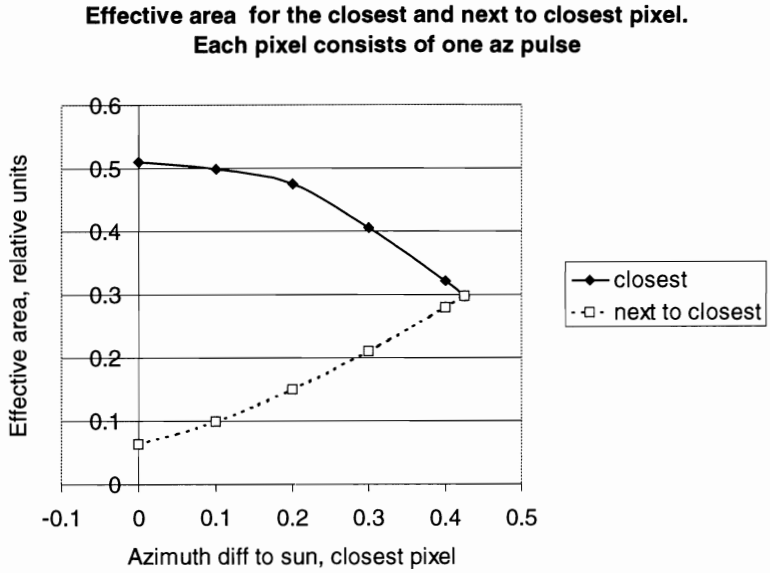

Fig 8. The effective antenna area occupied by the sun depends upon the angular distance to the sun. In elevation the radar is supposed to point at the centre of the sun

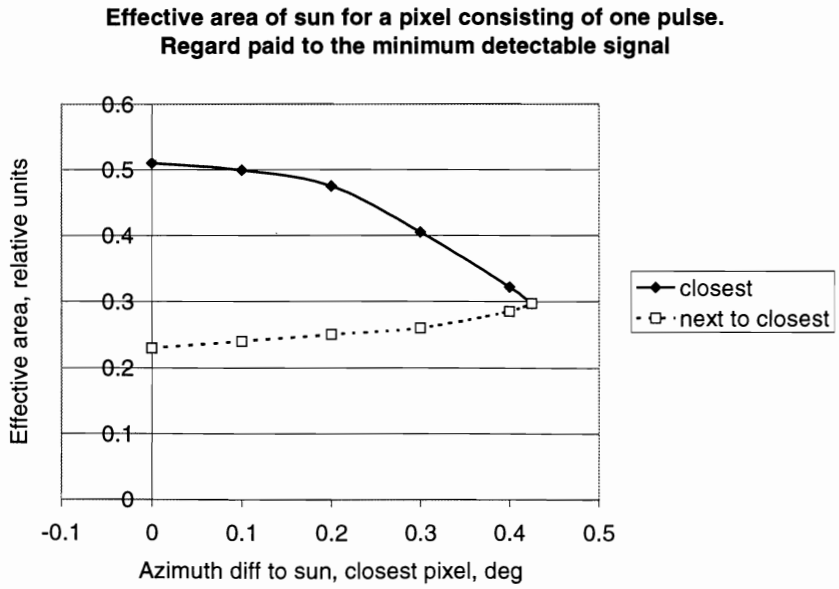

Fig. 9. Since the weakest sun signals fall below the radars minimum detectable signal, a larger effective area has been introduced for the azimuth next closest to the sun. The objective is to get better correspondence to the computed values of the sun intensity, see text.

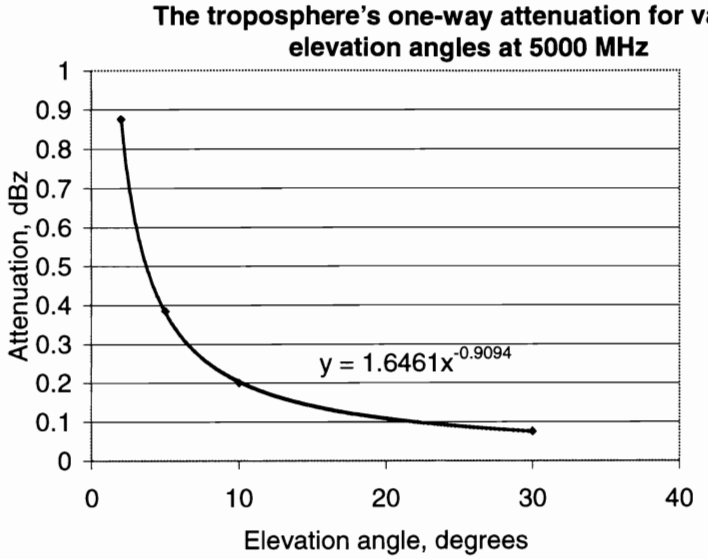

Fig. 10. The one-way attenuation of radiation passing through the atmosphere. Nathanson, 1969.

Working with routine data, the pixel values we get can be considered to have a resolution of one pulse width in elevation. In azimuth, however, every pixel contains six consecutive azimuth pulses. With our scan speed, 10 revolutions per minute, each pixel is should contain six azimuth pixels and six range bins. However, only one azimuth pulse is actually used for the pixel value. We assume that this pulse has the azimuth given in the polar data files the radar delivers. If also we assume that the elevation angle of the sun equals the antenna elevation angle we get

$$f(sun) = \int_{\alpha-sr}^{\alpha+sr} f(\alpha)d\alpha$$

Now we can write the antenna's effective area as a function of the angular distance to the sun (remember at the elevation angle of the sun)

$A_e = f(sun) * G * \lambda / 4\pi$

The sun emits S_flux watts/m^{2}Hz, and with a receiver band-width B the antenna thus receives

$P_{r\_sun} = A_e * B * S\_flux$

However, the solar flux is attenuated by the passage through the atmosphere and the wave-guide. The attenuation by the atmosphere, as given by Nathanson (1969) is shown in Fig. 10. Note that we are using elevations above 5°, and the attenuation here is much smaller than the one for nearly horizontal rays, which appear in the 'ordinary' use of weather radar for precipitation monitoring. Introducing these attenuations we get

$$p_{r\_sun} = A_e * B * S\_flux / L_{trop} * L_{wg} / 2 \qquad (5)$$

The wave-guide loss here is one-way, that is half the one used in the ordinary meteorological radar equation.

We must also note that solar observatories measure the unpolarized radiation, while our radars measure only the horizontally polarized part. Therefore

$$p_r\_sun = A_e * B * S\_flux / L_{trop} * L_{wg} \qquad (6)$$

If we have an observation of solar flux from a solar observatory we can thus compare it with the solar signal measured by our weather radars. Working with one radar, keeping the range r constant we can write the radar equation

$$p_r = const * Z$$

Since, if we measure against the sun we should expect

$$p_r = p_r\_sun$$

we get

$$p_r\_sun = const * Z$$

Multiplying by 10 and taking logarithms

$$10 * \log(S\_flux) = dBz + CONST \qquad (7)$$

dBz is the reflectivity of the sun measured by the radar at a given range. In this study 240 km has been used. Knowing the technical data, the value of *CONST* can be computed for each radar. For instance, the Norrköping radar has, with actual calibration factors, and for a sun elevation angle of 15^{o}

$$10 * \log(S\_flux) = dBz + 11.95$$

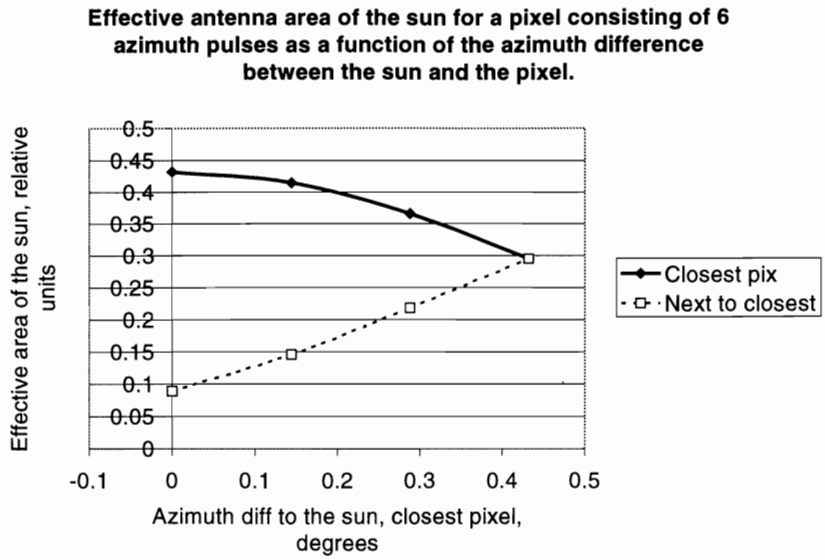

Fig. 11. Effective antenna area as a function of the angular difference to the sun for the azimuth closest and next closest to the sun. All available data used to compute the intensity value, see text.

A better pixel value should be obtained if all the azimuth pulses were used to compute the pixel value, Fig. 11. It is probable that the system will be developed to do this. If so, the pixel can be considered as an ellipsoid pulse, and with, as before, the effective area a function of the azimuth angle to the sun:

$$f(sun) = \frac{1}{6} * \sum_{1}^{6} \int_{\alpha-sr}^{\alpha+sr} f(\alpha) d\alpha$$

The preceding discussion is valid also here, all that has to be done is to use this formula for the effective area of the sun. Evidently, we get the maximum sun signal when we have three whole pulses to the left of the sun and three to the right. With the rate of revolution used, 1 revolution per 10 seconds, and the PRF 250, the angular distance between the pulses is 36/250=0.144°. Table 3, giving *f(sun)* as a function of the azimuth difference between the centres of the sun and pixel, uses this figure as unit. Since we generally record sun signals from two consecutive azimuths, the table gives areas for three consecutive azimuths.

Table 3. Effective area of the sun as a function of the azimuth angle to the sun for three consecutive (in azimuth) pulses.

Azi-muth no	Distance between centres of sun and azimuth no 0, degrees			
	0.000°	0.144°	0.288°	0.432°
-1	0.0892	0.0490	0.0240	0.0110
0	0.4323	0.4145	0.3653	0.2950
1	0.0892	0.1465	0.2180	0.2950

See also Fig. 11.

6. The interpolation of angles and intensity of the sun signal

The aim is to use the sun observations to get estimates of the accuracy of the radar's azimuth and elevation angle measurements. The angles to the sun are obtained from the routine SUN in the EWIS2 (Ericsson Weather Information System) software package. The resolution of the radar's observations is bounded by the resolution of the observations. We work with the polar volume data, where the resolution in azimuth is 359/419=0.8568° (each complete antenna revolution has 420 gates, 0 to 419). The antenna elevation scans permit a resolution of 0.2°. Therefore, the scan strategy contained 10 consecutive elevation angles with 0.2° spacing around a convenient elevation. We have used elevation angles centred somewhere between 7 and 20°. The reason for these comparatively low angles is the low solar elevations during our winter. As will be shown, neither the atmospheric attenuation nor the bending of the solar rays are serious at these angles, and moreover we have compensated for them.

With these figures we can expect a resolution of ±half the elevation step or ±0.1° in elevation and ±half the pixel width, or ±0.43° in azimuth. However, the sun is generally observed in at least two azimuths, and in several elevations. This permits interpolation, giving a higher expected resolution.

6.1 The bending of rays in a vertical plane

During the passage through the atmosphere, the rays are bent towards the earth. For elevation angles above 5° this atmospheric refraction or bending is given by Bean and Dutton (1969)

$$bend = 10^{-6} * N_o * cot\,(el_o)$$

N_o index of refraction at the surface

el_o angle of elevation at the surface, radians

For an angle of elevation of 10° this gives a bending of about 0.1°, for 20° about 0.05° and for 45° about 0.02°.

6.2 The interpolation of angles of elevation

As mentioned earlier, our radars permit a resolution of 0.2° in the vertical. The effective antenna area of the sun is given in Table 2 and Fig 8. If the sun is just between two elevation steps, the sun signal should be the same for both elevations, but lower than for an exact hit. If, on the other hand, the sun is exactly at one elevation (and thus 0.2° from the surrounding ones), Fig. 8 and Table 2 show that the relation between the area of the exact hit (S1 in the flow diagram) and the other (S2 in the flow diagram) should be 0.51/0.46. This gives a

difference of 0.48 dB. If the closest pulse is 0.05° and the next to closest 0.15° from the sun the relation should be 0.50/0.475 or 0.22 dB. Fitting a second degree polynomial to this figures gives Fig. 13 and the equation for interpolating the radar's elevation angle to the sun. This equation has been applied .It is always difficult to work with a small difference between two (relatively) large numbers. Nevertheless, it improves the resolution as well as the possibility to compare the elevations given by the radar with the astronomic data (including the bending of the rays) and thus give better estimates of the accuracy of the radar's elevation angles. An example is given in Fig. 14 from

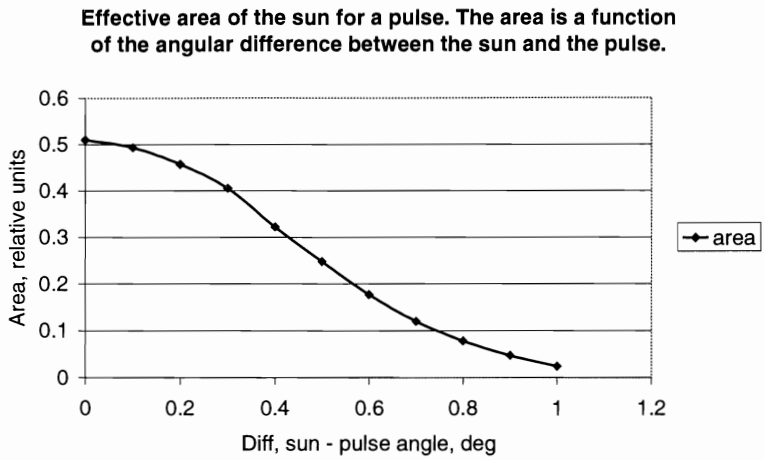

Fig. 12. The effective antenna area changes only little between 0.00 and 0.15°.

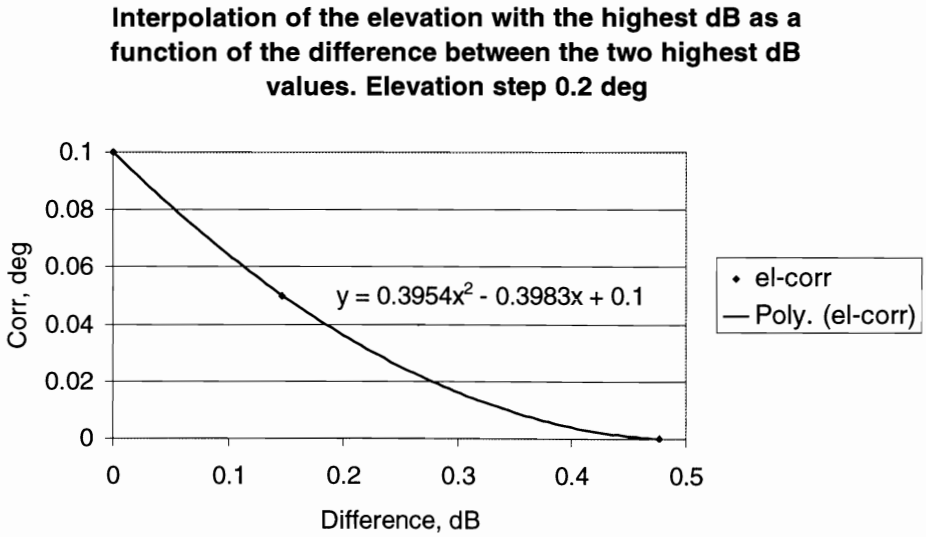

Fig. 13. The sign of corr depends upon the sign of the difference between the elevation angles. If the highest elevation has the maximum dBz, the sign is negative.

the Norrköping radar 22 Dec. 1999, 10:00 UTC. The vertical reflectivity profile of the sun fits the expected profile according to the equation on p 14

$P_r sun = A_e * B * S\_flux$

well, the main difference being that the observed curve is somewhat broader. The reason is that the weak sun signals at larger angle differences often fall below the minimum detectable signal, and the lowest values are thus often missing in the computation of observed mean values. Fig 15 repeats the observed curve at 10:48, but also shows the corresponding curves for 11:03 UTC. Here the sun is observed in two azimuths (181.64° and 182.50°), though only weakly in the latter. In azimuth 181.64° the observations suggest a maximum at 8.0°, but actually it is a weak minimum there. I have no explanation for this. Actually, this feature has been observed at all the radars which hitherto have been subject to this kind of study, but its occurrence is coupled to the individual radar. Radar Gotland, for instance has a much higher frequency than the Norrköping radar, and at the Gotland radar the minimum is often much more pronounced than in Fig 15. Since it's frequency thus is coupled to the radar, it can hardly be due to the soft-ware or inhomogenities in the radiation from the sun, but sooner to the hardware of the radar, for instance the antenna. It may be an artefact, due to the fact that we do not know which of the six azimuth bins of the azimuth gate the radar is actually using.

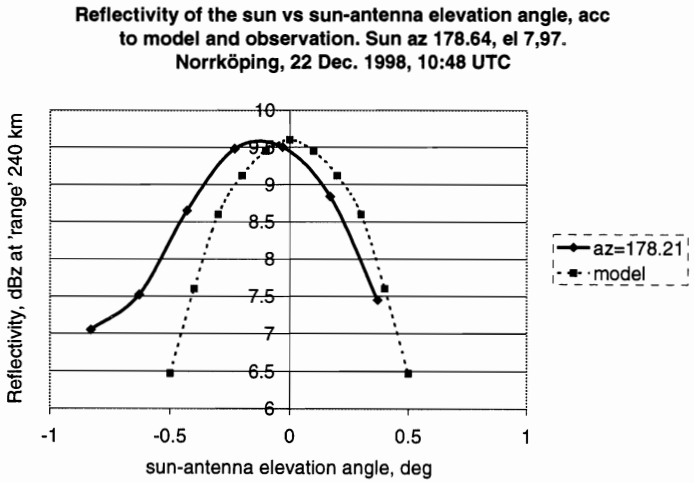

Fig. 14. The shape of the observed curve is very similar to the expected shape. The displacement, about -0.15°,may be due to the atmospheric refraction. The observed curve is broader. The explanation may be that the weaker sun signals are below the minimum detectable level, and the compensation for this in Fig 9 is not perfect.

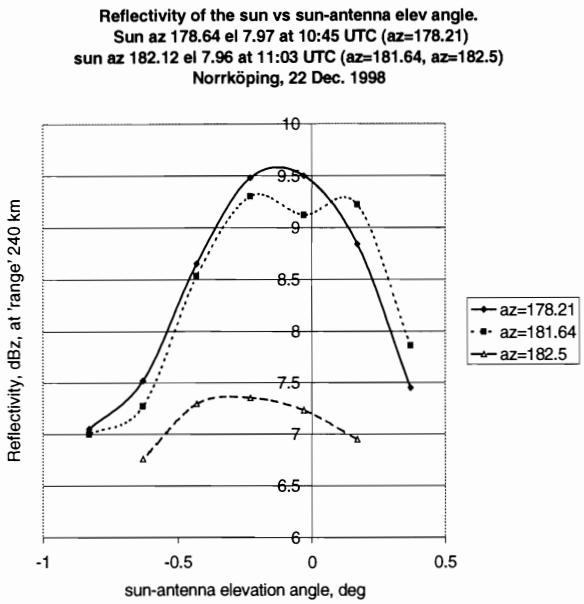

Fig. 15. 15 minutes after the time of the preceding Fig., the curves are similar, but there is a conspicuous dip in one of them.

6.3 The interpolation of angles of azimuth

Six azimuth pulses are collected for each pixel. However, only one is used. We will assume that the used one is centred just at the azimuth given in the polar volumes.

We have assumed that in elevation the antenna points directly into the centre of the sun. The effective areas as a function of the angle to the sun are given in Fig. 8. This Fig. gives the areas for two pulses, the one closest to the sun and the one next to closest. Since the dBz values recorded are proportional to the log(area) values, we can use this Fig. to interpolate the azimuth of the sun as well as it's reflectivity. The interpolation of the azimuth angles proceeds in the same way as the interpolation of elevation angles, but with one exception. Due to the coarser resolution in azimuth (0.86^{o}), several pixels, which only partially hit the sun, get signals below the minimum detectable signal. I have paid regard to this in Fig 9, which shows the effective antenna area as a function of the azimuth difference to the sun (supposing the radar points into the elevation of the sun.). Comparing to Fig. 8, the effective area of the pixel next to closest to the sun is larger. This increases the expected signal, which is just what occurs when the weakest signals do not reach the minimum detectable signal and therefore are excluded from the computations of the arithmetic mean. The difference in signal between the two pixels is determined by the difference of their effective areas. Thus, if index 1 denotes the pixel closest to the sun (S1 in the flow diagram), and index 3 the pixel next closest to the sun (S3 in the flow diagram on p 23), the difference in received signal in dB is

$\Delta dB = 10*log(y_1 / y_3)$

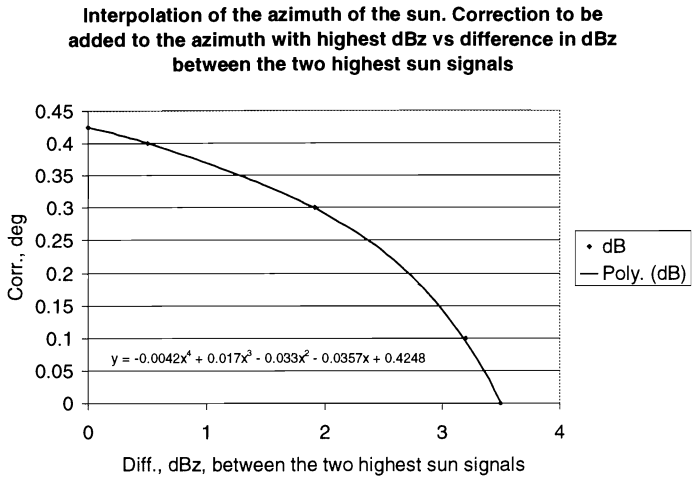

Fig. 16. The sign of the correction depends upon the difference between the azimuths. If the azimuth with the highest dB is larger than the azimuth with the next to highest then the correction is negative. If both azimuths have the same dB, the corrected azimuth is the arithmetic mean of the two azimuths.

These values are plotted in Fig. 16, together with the interpolation equation. Here we have the same difficulty as in the interpolation of angle of elevation, namely the uncertainty of working with a small difference between two (relatively) large numbers. However, the resolution is increased. So is also the possibility to compare the azimuths given by the radar with the astronomic data.

6.4 Interpolating the intensity of the sun signal

What we want is the intensity of the sun signal when the antenna is pointing directly into the sun. In Fig. 17 this is the y value at x=0. In analogy to the azimuth interpolation, we can interpolate the intensity in the following way. In Fig. 9 the x value 0.2 indicates that the closest pixel is 0.2^{o} from the sun. The next to closest is $0.2-0.85=-0.65^{o}$ and is plotted at the same x, curve 'next to closest'. The expected difference in signal intensity between these two pixels is

10*log(0.48/0.26)=2.7 dB, and the correction to be added to the highest reading is given by the y values at x=0 and x=0.2 of the curve 'closest', that is as 10*log(0.51/0.48)= 0.3 dB. These corrections are given in Fig. 17, together with the equation for the interpolations.

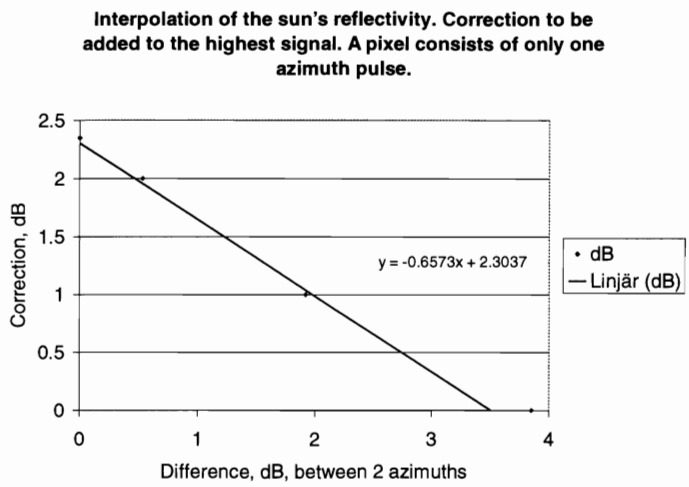

Fig. 17. Interpolation of the intensity of the sun radiation.

7. How the observations were performed

The flow diagram gives an overview of the work procedure.

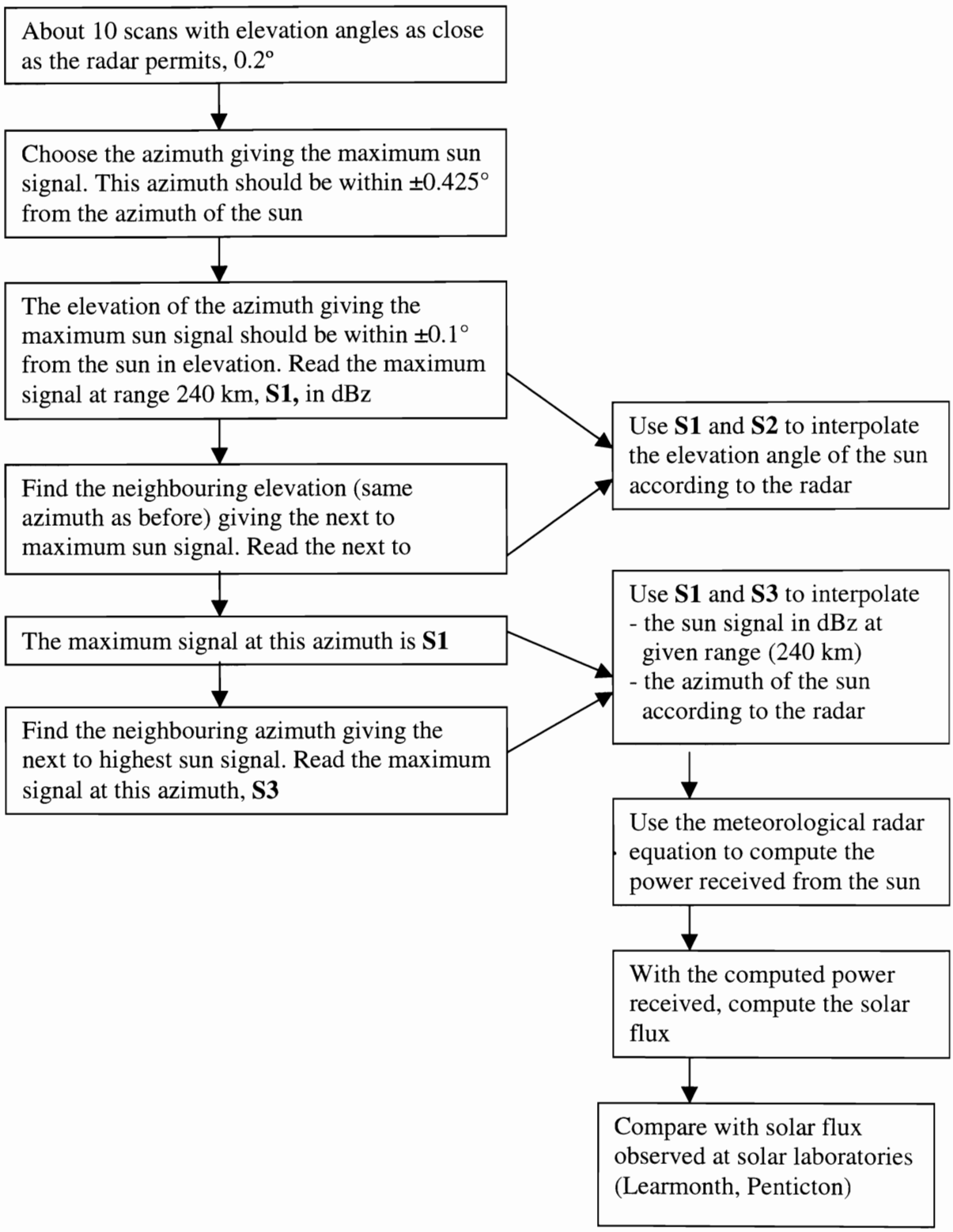

8. Results obtained with measurements against the sun

The preceding results have been applied on some radars. We will discuss them for two radar separately.

8.1 The Gotland radar

One peculiarity of this radar is often evident. The vertical profile of reflectivity (reflectivity against antenna elevation angle) is often not as smooth as expected. The dips in Fig. 18 are not easy to explain. It may be due to the azimuth angle selection. Of the six pulses comprising the azimuth pixel, only one is used. We have assumed that the central one is used, i. e. the one having just the azimuth given in the polar data volume. The six pulses span an azimuth of 0.86°. If another one is used, it could be 0.43° displaced from the 'nominal' value and cause such a dip. In any case, this phenomena affects our estimates of angles as well as signal intensity, As to angles, if the pulse used is chosen by a random process, it should not affect average values, but cause a larger spread. As to intensity, it is not clear how it should affect the interpolated values.

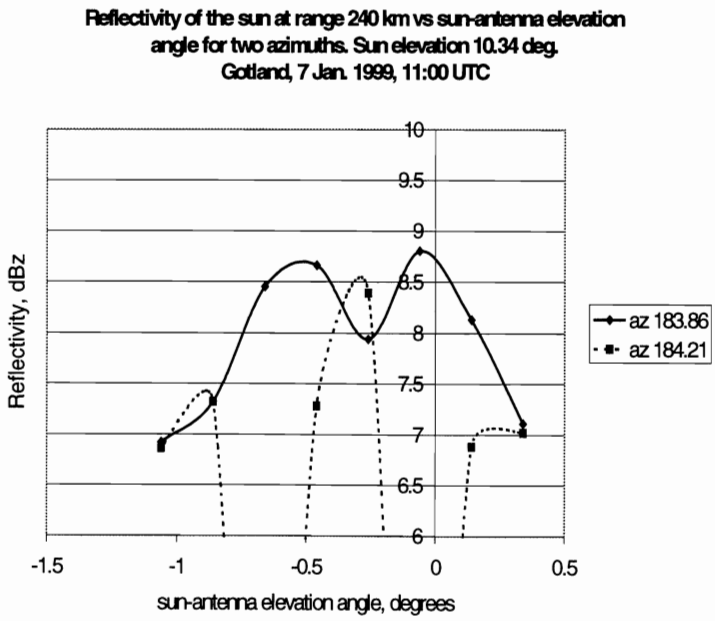

Fig. 18. Irregular sun profiles. Note one dip of az 183.86 and two dips of az 184.21, where the sun appears weaker, and the sun signal disappears at sun-antenna elevations of -0.06 and -0.66

8.1.1 The measurement of angles

Fig. 19 shows that the azimuth readings differ by about 1° from the astronomic.

Fig. 20 shows that the radar gives a somewhat too high elevation angle. No trend is discernible, but this may be due the comparatively large spread of the data. A trend should be expected if the antenna axis is mounted on a not quite horizontal table. In such a case, this trend should be cyclic, a sine curve. If there really is such a trend, it

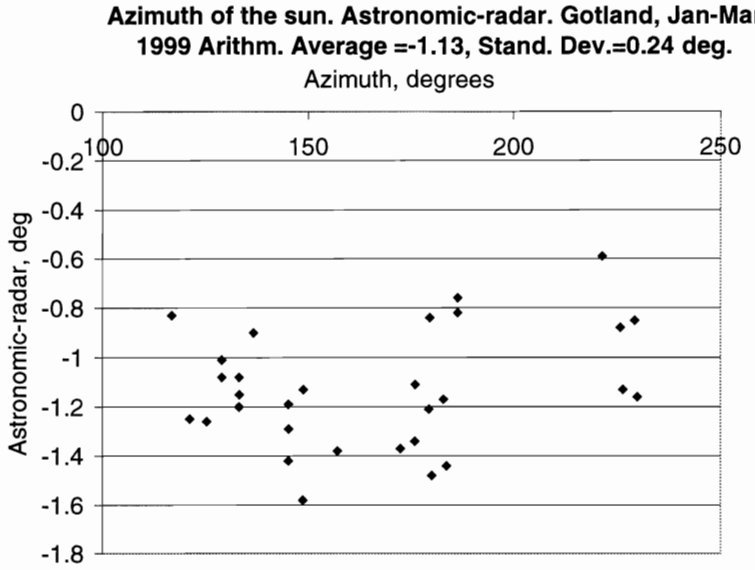

Fig. 19. The Gotland radar consistently gives an about 1^{o} too large azimuth angle to the sun

should be discernible with a larger span in azimuth, which is possible to realise during summer.

8.1.2 The intensity measurements

As shown by Fig. 21, the observed values are fairly close to the expected ones. Fitting a regression line to the observed values gives

*y=2.67*x - 49*

with an explained variance of 0.65. For the sfu interval here the values agree well. With the low span of the values, only about 2 dB, we cannot expect a very good fit of the slope. The average of reflectivity and solar flux are 10.40 and 22.34 respectively. The latter figure gives an expected dBz of 10.41 (see the equation on Fig. 21).

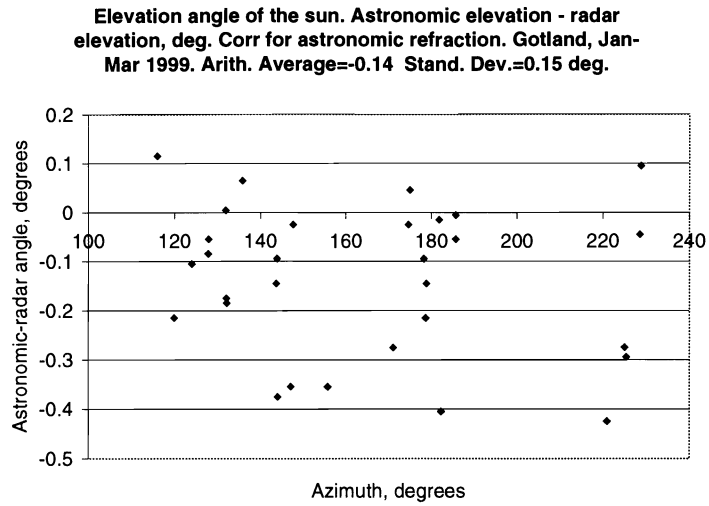

Fig. 20. The Gotland radar gives somewhat too high elevation angles. Any possible trend of the data is shadowed by their large spread.

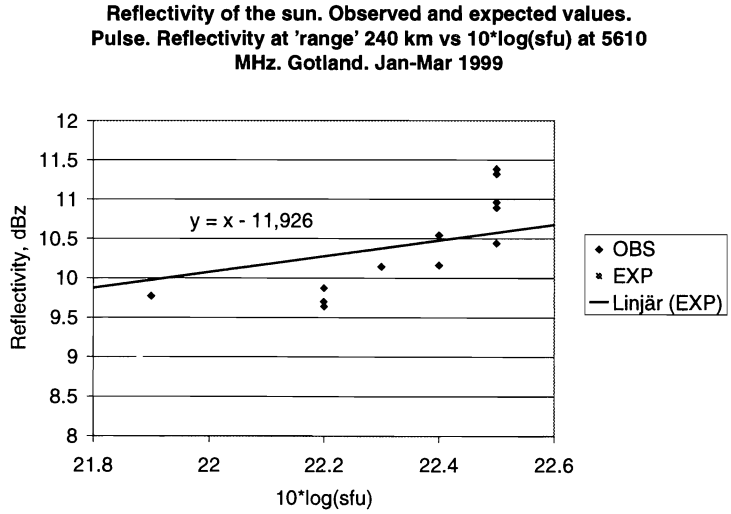

Fig. 21. The reflectivity of the sun according to the Gotland radar versus observations of the solar flux at 5610 MHz from Learmonth, Australia. The line gives the expected values of dBz according to the radar equation. sfu=solar flux unit.
1 sfu = $10^{-22}Wm^{-2}Hz^{-1}$.

8.2 The Norrköping radar

The Norrköping radar shows much smoother profiles of reflectivity against antenna elevation angle than the Gotland radar. Though also Norrköping has some hard-to-explain peculiarities, they are not at all as severe. This is probably why the Norrköping angles show a less spread from the astronomic. Also the average deviations are smaller for Norrköping, Fig 22 and 23. As to the intensity

measurements, the Norrköping radar appers to be about 1.5 dB below the expected values, Fig. 24.

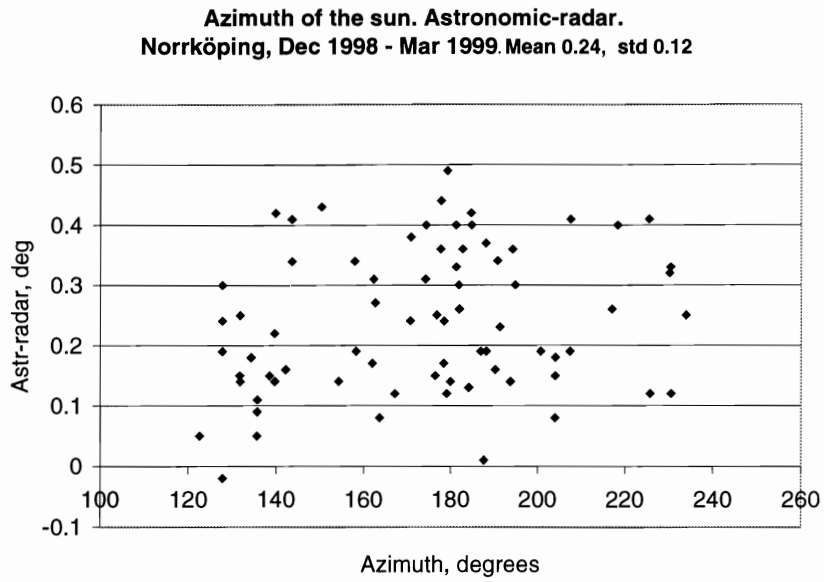

Fig. 22. The azimuth angles from the Norrköping radar agree better with the astronomic angles

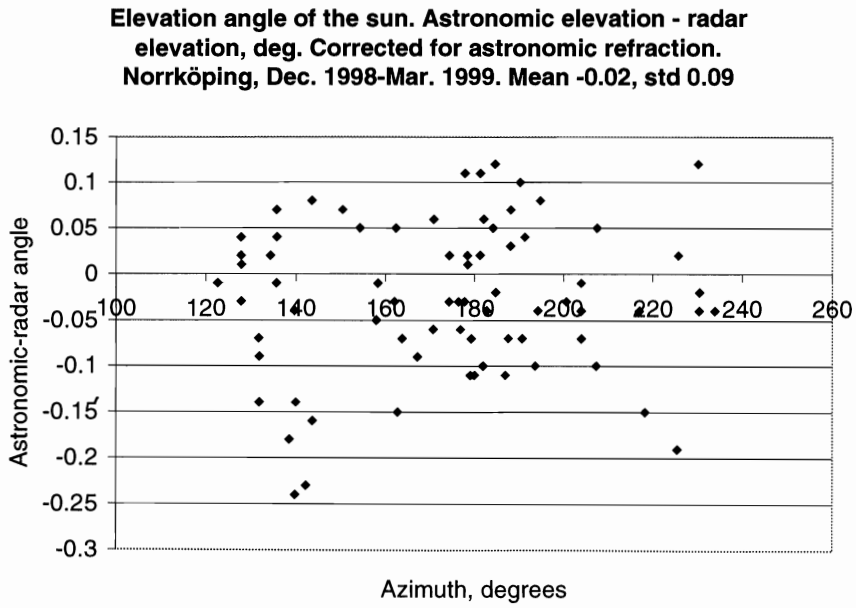

Fig. 23. The elevation angles from the Norrköping radar also agree better with the astronomic angles. There may be a trend. A larger azimuth span can show if that is the case.

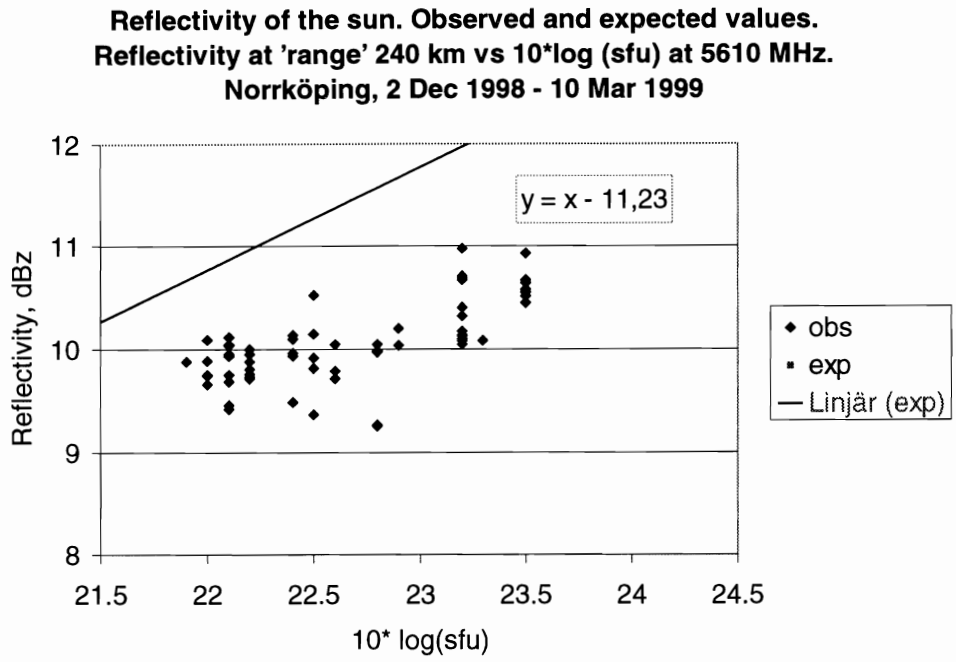

Fig. 24. The reflectivity of the sun according to the Norrköping radar versus observations of the solar flux at 5610 MHz from Learmonth, Australia. The line gives the expected values of dBz according to the radar equation.
The dBz values of the Norrköping radar are about 1,5 dBz below the expected ones.
sfu=solar flux unit.
1 sfu = $10^{-22} Wm^{-2}Hz^{-1}$.

9. Conclusions

It is possible to use the sun for several checks of a weather radar's condition. This works shows that is very easy for the meteorological operator to check the horisontal alignment of the antenna using the sun echo. It is also possible for him/her to check the vertical alignment, though this requires a special scan scheme. Also the intensity measurements may be checked if the measurements of the sun radiation in the actual frequencies are known. Such data are available from solar observatories.
More satisfactory should be to implement a strategy for these tasks in the ordinary scanning routines. Actually, such a strategy is now introduced in the Swedish weather radar network.

10. Acknowledgements: This work was supported by the European Community, Contract N° ENV4-CT97-0484. Thanks are also due to the Dominion Radio Astrophysical Observatory and the Australian Space Forecast Centre, especially Richard Thompson, for valuable discussions and data.

11. References:

Battan, L.J., 1973: Radar Observation of the Atmosphere. *Chicago Press,* Chicago.

Bean, B.R. and E.J. Dutton, 1968: Radio Meteorology. *Dover Books,* New York.

Croom, D.L. and C. Eng, 1973: Sun as a broadband source for tropospheric attenuation measurements at millimetre wavelengths. *Proc. IEE,* **120**, 1200-1206.

Dahlberg, L., 1996: Analysis of hardware and software differences in the NORDRAD Weather Radars and how these will affect calibration and measurements of the dBZ-values. *RadMet AB,* Mölndal.

Frush, C.L., 1984: Using the Sun as a calibration aid in multiple parameter meteorological radars. *Preprints, 22nd Conf. Radar Meteor.,* 10-13 Sep. 1984, Zűrich, Switzerland, 306-311.

Nathanson, F.E., 1969: Radar design Principles. *McGraw-Hill Book Company,* 626 p.

Pratte, F., R. Gagnon, B. Lewis and C. Frush, 1995: Application of lunar echo to weather radar calibrations. *Preprints, 27nd Conf. Radar Meteorology,* Vail, Colorado, Oct. 9-13, 1995, 142-144.

Probert-Jones, J.R., 1962: The radar equation in meteorology. *Quart. J. Roy. Meteor. Soc.,* **88**, 485-495.

Whiton, R.C., P.L. Smith Jr and A.C. Harbruck, 1976: Calibration of weather radar systems using the sun as a radio source. *Preprints, 17th Conf. Radar Meteor.,* Boston, Seattle, Washington, Oct. 26-29, 1976, 60-65.

APPENDIX

Technical data for the Ericsson Doppler weather radar

Antenna	
Diameter	4.2 m
Gain	44.9 dB
Beam Width	0.9°
Polarization	Linear horizontal
Radome	
Diameter	6.7 m
Transmission loss	<0.2 dB
Antenna servo	
Azimuth movement	360° up to 6 rpm
Azimuth accuracy	0.2°
Elevation movement	-1° to 90°
Elevation accuracy	0.1°
Transmitter	
Frequency	5600 – 5650 MHz
Sensitivity	Better than –109 dBm (non-Doppler) Better than –114 dBm (Doppler)
Dynamic range	>85 dB (log receiver), > 87 dB (linear receiver with IAGC)
Signal processor	
A/D conversion	8 bits
Sampling rate	333 m nominally (non-Doppler), 83 m (Doppler)
Range integration	6 samples(non-Doppler), 12 samples (Doppler)
Instrumented range	480 km (non-Doppler), 120 km (Doppler)
Range resolution	2 km (non-Doppler), 1 km (Doppler)
Azimuth integration	1-64 pulses (non-Doppler), 2*32 pulses FFT (Doppler)
Data outputs	Reflectivity, radial velocity (Doppler only), spctrum width (Doppler only)
Data corrections	Range dependence, atmospheric attenuation and rain attenuation
Data resolution	Reflectivity 0.4 dBz, velocity 0.375 m/s, spectrum width 2 m/s classes
Data coverage	Reflectivity-30 t +72 dBz, velocity –48 to +48 m/s, spectrum width 4 classes: 0-2, 2-4, 4-6 and >6 m/s
Data accuracy	Reflectivity 1 dB Velocity <0.3 m/s 10 dB S/N, <0.6 m/s 0 dB S/N

SMHIs publications

SMHI publishes six report series. Three of these, the R-series, are intended for international readers and are in most cases written in English. For the others the Swedish language is used.

Names of the Series	**Published since**
RMK (Report Meteorology and Climatology)	1974
RH (Report Hydrology)	1990
RO (Report Oceanography)	1986
METEOROLOGI	1985
HYDROLOGI	1985
OCEANOGRAFI	1985

Earlier issues published in serie RMK

1 Thompson, T., Udin, I., and Omstedt, A. (1974)
Sea surface temperatures in waters surrounding Sweden.

2 Bodin, S. (1974)
Development on an unsteady atmospheric boundary layer model.

3 Moen, L. (1975)
A multi-level quasi-geostrophic model for short range weather predictions.

4 Holmström, I. (1976)
Optimization of atmospheric models.

5 Collins, W.G. (1976)
A parameterization model for calculation of vertical fluxes of momentum due to terrain induced gravity waves.

6 Nyberg, A. (1976)
On transport of sulphur over the North Atlantic.

7 Lundqvist, J.-E., and Udin, I. (1977)
Ice accretion on ships with special emphasis on Baltic conditions.

8 Eriksson, B. (1977)
Den dagliga och årliga variationen av temperatur, fuktighet och vindhastighet vid några orter i Sverige.

9 Holmström, I., and Stokes, J. (1978)
Statistical forecasting of sea level changes in the Baltic.

10 Omstedt, A., and Sahlberg, J. (1978)
Some results from a joint Swedish-Finnish sea ice experiment, March, 1977.

11 Haag, T. (1978)
Byggnadsindustrins väderberoende, seminarieuppsats i företagsekonomi, B-nivå.

12 Eriksson, B. (1978)
Vegetationsperioden i Sverige beräknad från temperaturobservationer.

13 Bodin, S. (1979)
En numerisk prognosmodell för det atmosfäriska gränsskiktet, grundad på den turbulenta energiekvationen.

14 Eriksson, B. (1979)
Temperaturfluktuationer under senaste 100 åren.

15 Udin, I., och Mattisson, I. (1979)
Havsis- och snöinformation ur datorbearbetade satellitdata - en modellstudie.

16 Eriksson, B. (1979)
Statistisk analys av nederbördsdata. Del I. Arealnederbörd.

17 Eriksson, B. (1980)
Statistisk analys av nederbördsdata. Del II. Frekvensanalys av månadsnederbörd.

18 Eriksson, B. (1980)
Årsmedelvärden (1931-60) av nederbörd, avdunstning och avrinning.

19 Omstedt, A. (1980)
A sensitivity analysis of steady, free floating ice.

20 Persson, C., och Omstedt, G. (1980)
En modell för beräkning av luftföroreningars spridning och deposition på mesoskala.

21 Jansson, D. (1980)
Studier av temperaturinversioner och vertikal vindskjuvning vid Sundsvall-Härnösands flygplats.

22 Sahlberg, J., and Törnevik, H. (1980)
A study of large scale cooling in the Bay of Bothnia.

23 Ericson, K., and Hårsmar, P.-O. (1980)
Boundary layer measurements at Klock-rike. Oct. 1977.

24 Bringfelt, B. (1980)
A comparison of forest evapotranspiration determined by some independent methods.

25 Bodin, S., and Fredriksson, U. (1980)
Uncertainty in wind forecasting for wind power networks.

26 Eriksson, B. (1980)
Graddagsstatistik för Sverige.

27 Eriksson, B.(1981)
Statistisk analys av nederbördsdata. Del III. 200-åriga nederbördsserier.

28 Eriksson, B. (1981)
Den "potentiella" evapotranspirationen i Sverige.

29 Pershagen, H. (1981)
Maximisnödjup i Sverige (perioden 1905-70).

30 Lönnqvist, O. (1981)
Nederbördsstatistik med praktiska tillämpningar.
(Precipitation statistics with practical applications.)

31 Melgarejo, J.W. (1981)
Similarity theory and resistance laws for the atmospheric boundary layer.

32 Liljas, E. (1981)
Analys av moln och nederbörd genom automatisk klassning av AVHRR-data.

33 Ericson, K. (1982)
Atmospheric boundary layer field experiment in Sweden 1980, GOTEX II, part I.

34 Schoeffler, P. (1982)
Dissipation, dispersion and stability of numerical schemes for advection and diffusion.

35 Undén, P. (1982)
The Swedish Limited Area Model. Part A. Formulation.

36 Bringfelt, B. (1982)
A forest evapotranspiration model using synoptic data.

37 Omstedt, G. (1982)
Spridning av luftförorening från skorsten i konvektiva gränsskikt.

38 Törnevik, H. (1982)
An aerobiological model for operational forecasts of pollen concentration in the air.

39 Eriksson, B. (1982)
Data rörande Sveriges temperaturklimat.

40 Omstedt, G. (1984)
An operational air pollution model using routine meteorological data.

41 Persson, C., and Funkquist, L. (1984)
Local scale plume model for nitrogen oxides. Model description.

42 Gollvik, S. (1984)
Estimation of orographic precipitation by dynamical interpretation of synoptic model data.

43 Lönnqvist, O. (1984)
Congression - A fast regression technique with a great number of functions of all predictors.

44 Laurin, S. (1984)
Population exposure to SO and NO_x from different sources in Stockholm.

45 Svensson, J. (1985)
Remote sensing of atmospheric tempera-ture profiles by TIROS Operational Vertical Sounder.

46 Eriksson, B. (1986)
Nederbörds- och humiditetsklimat i Sverige under vegetationsperioden.

47 Taesler, R. (1986)
Köldperioden av olika längd och förekomst.

48 Wu Zengmao (1986)
Numerical study of lake-land breeze over Lake Vättern, Sweden.

49 Wu Zengmao (1986)
Numerical analysis of initialization procedure in a two-dimensional lake breeze model.

50 Persson, C. (1986)
Local scale plume model for nitrogen oxides. Verification.

51 Melgarejó, J.W. (1986)
An analytical model of the boundary layer above sloping terrain with an application to observations in Antarctica.

52 Bringfelt, B. (1986)
Test of a forest evapotranspiration model.

53 Josefsson, W. (1986)
Solar ultraviolet radiation in Sweden.

54 Dahlström, B. (1986)
Determination of areal precipitation for the Baltic Sea.

55 Persson, C. (SMHI), Rodhe, H. (MISU), De Geer, L.-E. (FOA) (1986)
The Chernobyl accident - A meteorological analysis of how radionucleides reached Sweden.

56 Persson, C., Robertson, L. (SMHI), Grennfelt, P., Kindbom, K., Lövblad, G., och Svanberg, P.-A. (IVL) (1987)
Luftföroreningsepisoden över södra Sverige 2 - 4 februari 1987.

57 Omstedt, G. (1988)
An operational air pollution model.

58 Alexandersson, H., Eriksson, B. (1989)
Climate fluctuations in Sweden 1860 - 1987.

59 Eriksson, B. (1989)
Snödjupsförhållanden i Sverige - Säsongerna 1950/51 - 1979/80.

60 Omstedt, G., Szegö, J. (1990)
Människors exponering för luftföroreningar.

61 Mueller, L., Robertson, L., Andersson, E., Gustafsson, N. (1990)
Meso-γ scale objective analysis of near surface temperature, humidity and wind, and its application in air pollution modelling.

62 Andersson, T., Mattisson, I. (1991)
A field test of thermometer screens.

63 Alexandersson, H., Gollvik, S., Meuller, L. (1991)
An energy balance model for prediction of surface temperatures.

64 Alexandersson, H., Dahlström, B. (1992)
Future climate in the Nordic region - survey and synthesis for the next century.

65 Persson, C., Langner, J., Robertson, L. (1994)
Regional spridningsmodell för Göteborgs och Bohus, Hallands och Älvsborgs län. (A mesoscale air pollution dispersion model for the Swedish west-coast region. In Swedish with captions also in English.)

66 Karlsson, K.-G. (1994)
Satellite-estimated cloudiness from NOAA AVHRR data in the Nordic area during 1993.

67 Karlsson, K-G. (1996)
Cloud classifications with the SCANDIA model.

68 Persson, C., Ullerstig, A. (1996)
Model calculations of dispersion of lindane over Europe. Pilot study with comparisons to measurements around the Baltic Sea and the Kattegat.

69 Langner, J., Persson, C., Robertson, L., and Ullerstig, A. (1996)
Air pollution Assessment Study Using the MATCH Modelling System. Application to sulfur and nitrogen compounds over Sweden 1994.

70 Robertson, L., Langner, J., Engardt, M. (1996)
MATCH - Meso-scale Atmosperic Transport and Chemistry modelling system.

71 Josefsson, W. (1996)
Five years of solar UV-radiation monitoring in Sweden.

72 Persson, C., Ullerstig, A., Robertson, L., Kindbom, K., Sjöberg, K. (1996)
The Swedish Precipitation Chemistry Network. Studies in network design using the MATCH modelling system and statistical methods.

73 Robertson, L. (1996)
Modelling of anthropogenic sulfur deposition to the African and South American continents.

74 Josefsson, W. (1996)
Solar UV-radiation monitoring 1996.

75 Häggmark, L., Ivarsson, K.-I. (SMHI), Olofsson, P.-O. (Militära vädertjänsten). (1997)
MESAN - Mesoskalig analys.

76 Bringfelt, B, Backström, H, Kindell, S, Omstedt, G, Persson, C, Ullerstig, A. (1997)
Calculations of PM-10 concentrations in Swedish cities- Modelling of inhalable particles

77 Gollvik, S. (1997)
The Teleflood project, estimation of precipitation over drainage basins.

78 Persson, C., Ullerstig, A. (1997)
Regional luftmiljöanalys för Västmanlands län baserad på MATCH modell-beräkningar och mätdata - Analys av 1994 års data

79 Josefsson, W., Karlsson, J.-E. (1997)
Measurements of total ozone 1994-1996.

80 Rummukainen, M. (1997)
Methods for statistical downscaling of GCM simulations.

81 Persson, T. (1997)
Solar irradiance modelling using satellite retrieved cloudiness - A pilot study

82 Langner, J., Bergström, R. (SMHI) and Pleijel, K. (IVL) (1998)
European scale modelling of sulfur, oxidized nitrogen and photochemical oxidants. Model development and evaluation for the 1994 growing season.

83 Rummukainen, M., Räisänen, J., Ullerstig, A., Bringfelt, B., Hansson, U., Graham, P., Willén, U. (1998)
RCA - Rossby Centre regional Atmospheric climate model: model description and results from the first multi-year simulation.

84 Räisänen, J., Döscher, R. (1998)
Simulation of present-day climate in Northen Europé in the HadCM2 OAGCM.

85 Räisänen, J., Rummukainen, M., Ullerstig, A., Bringfelt, B., Ulf Hansson, U., Willén, U. (1999)
The First Rossby Centre Regional Climate Scenario - Dynamical Downscaling of CO_2-induced Climate Change in the HadCM2 GCM.

86 Rummukainen, Markku. (1999)
On the Climate Change debate

87 Räisänen, Jouni (2000)
CO_2-induced climate change in northern Europé: comparison of 12 CMIP2 experiments.

88 Engardt, Magnuz (2000)
Sulphur simulations for East Asia using the MATCH model with meteorological data from ECMWF.

89 Persson, Thomas (2000)
Measurements of Solar Radiation in Sweden 1983-1998

90 Daniel B. Michelson, Tage Andersson
Swedish Meteorological and Hydrological Institute (2000)
Jarmo Koistinen, Finnish Meteorological Institute
Christopher G. Collier, Telford Institute of Environmental Systems, University of Salford
Johann Riedl, German Weather Service
Jan Szturc, Instiute of Meteorology and Water Management
Uta Gjertsen, The Norwegian Meteorological Institute
Aage Nielsen, Danish Meteorological Institute
Søren Overgaard, Danish Meteorological Institute
BALTEX Radar Data Centre Products and their Methodologies

91 Josefsson, Weine (2000)
Measurements of total ozone 1997 – 1999

92 Andersson, Tage (2000)
Boundary clear air echos in southern Sweden

SMHI
Swedish Meteorological and Hydrological Institute
SE 601 76 Norrköping, Sweden.
Tel +46 11-495 80 00. Fax +46 11-495 80 01

ISSN 0347-2116